DOI: https://doi.org/10.14311/TPFM.2023.009

MIXING CHARACTERISTICS OF A MAGNETICALLY DRIVEN RUSHTON TURBINE IN AN UNBAFFLED STIRRED TANK REACTOR

K. Idžakovičová [1, 2, 3], J. Haidl [2], O. Gebouský [2, 3], M. Isoz [1, 4]

[1] **Czech Academy of Sciences, Institute of Thermomechanics, Dolejškova 5, Prague 182 00, Czech Republic**

[2] **Czech Academy of Sciences, Institute of Hydrodynamics, Pod Patankou 30/5, Prague 160 00, Czech Republic**

[3] **Department of Chemical Engineering, Faculty of Chemical Engineering, University of Chemistry and Technology, Technická 5, Prague 166 28, Czech Republic**

[4] **Department of Mathematics, Faculty of Chemical Engineering, University of Chemistry and Technology, Technická 5, Prague 166 28, Czech Republic**

Abstract

The standard and well-researched stirred vessel configuration comprises a tank equipped with one or more impellers positioned in the vessel's axis and multiple wall-mounted baffles preventing the central vortex creation. However, particular industries, such as biotechnology, have an increased need for a sterile environment that often results in the usage of atypical stirred vessel configurations. An example of a commonly equipped atypical stirred vessel is an unbaffled stirred tank with an eccentric magnetically driven impeller. However, there is only a little knowledge about the mixing characteristics of such designs. In this work, we list experimental results for both the standard and atypical stirred vessel configurations. Furthermore, we present a CFD model of the atypical configuration. The model is used to calculate its mixing characteristics that are subsequently compared against our experimental results. It is shown that for the liquid height (H) to the vessel diameter (T) ratio $H/T \lesssim 1.2$, the characteristics of both the standard and atypical designs coincide. For higher liquid heights (i) the characteristics of the atypical design decrease dramatically, and (ii) the characteristics estimates based on approaches developed for the standard configuration become unreliable.

Keywords: stirred vessel, eccentric impeller, unbaffled tank, CFD, OpenFOAM, experiment

1 Introduction

Stirred vessels are used in many industry branches as they help to equally distribute individual components within the solution [1]. This process is typically done in cylindrical tanks equipped with two to four baffles and one or more impellers positioned in the vessel's axis. The presence of baffles prevents the central vortex formation, thus significantly enhancing mixing characteristics of the vessel and reducing the time that it takes to have a fully homogenized solution [2].

For stirred vessels used in the pharmaceutical or biotechnological industry, an emphasis is often being made on a pure and sterile environment. Tank baffles as well as other internals are often missing in these configurations in order to improve tank cleanability. To maintain the tank mixing characteristics, alternative approaches compensating the adverse effect of missing internals are sought. For example, an efficient way to eliminate the central vortex formation is to position the impeller eccentrically [3]. Furthermore, in case of the need for a highly sterile environment, the impeller can be positioned near the tank wall, enabling the use of a magnetically coupled drive. In such a configuration, the vessel can be hermetically sealed, which makes it attractive especially for pharmaceutical bioreactors. As a result, unbaffled stirred tanks with eccentrical, magnetically driven impellers are already offered by several leading equipment manufacturers [4]. However, the design of such vessels is far from the standard, well characterized, configuration, hence non-standard mixing properties are to be expected.

Currently, there are a few studies done for the unbaffled configurations – examples can be found in works of Yu et al. [5], Galletti et al. [6] and Ram et al. [3]. One reference can be also found for the magnetically driven impeller in a baffled tank [7]. However, no experimental data can be found in the open literature for the unbaffled tank with a magnetically driven impeller. Due to the lack of research, the vessel designs are mostly done as a trial and error cases based on standard (centric) geometries and deficient computational results. As stirred bioreactors are prevalent in

pharmaceutical processes, there is a significant need to have a reliable and fast tool for vessel design and characterization of its hydrodynamics under various operational conditions.

The goal of this work is to present an economic yet reliable computational model of the unbaffled stirred tank with the eccentrical, magnetically driven, impeller. The mixing time $\theta_{0.95}$ is used as the representative characteristics. The model is verified against experimental results measured in the work. The mathematical model is created using Computational Fluid Dynamics (CFD) open-source library OpenFOAM [8]. The experimental and computational results are provided for both the *atypical* (unbaffled) and the *standard* (fully-baffled) vessel to enable a direct comparison of both configurations' characteristics.

2 Experimental setup

The experiments were performed using a modular PMMA cylindrical tank of diameter $T = 390$ mm and height of 700 mm equipped with a dished bottom. The modular configuration allowed for measurements with atypical (unbaffled) as well as standard (fully-baffled) geometries, see Fig 1. The wall of the tank was supplied with six openings that are used for the placement of measuring probes and the injection of tracers. The Rushton turbines with diameters D of 60, 80 and 100 mm were used for the measurements. Additional turbine parameters and denotations are summarized in Fig. 1d. The stepper motor was used for the impeller drive and speed control.

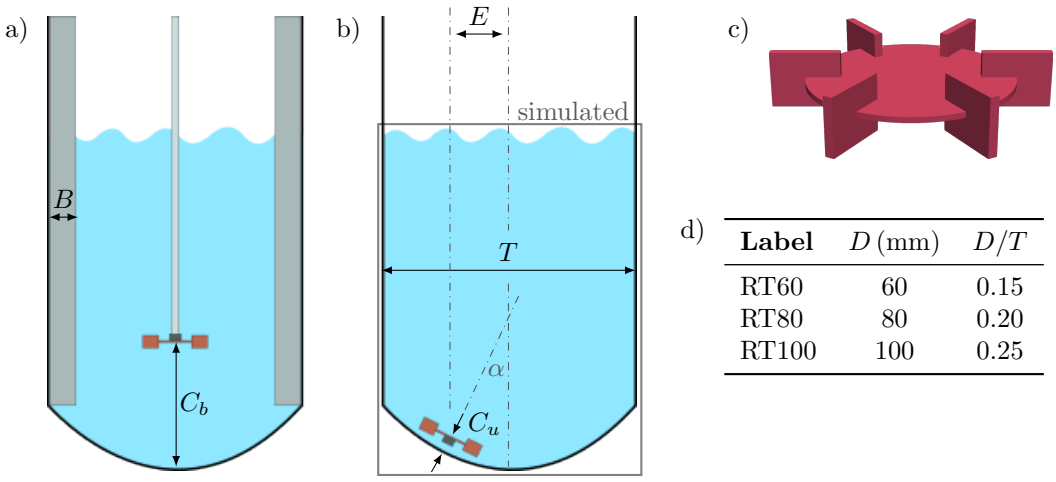

d)

Label	D (mm)	D/T
RT60	60	0.15
RT80	80	0.20
RT100	100	0.25

Figure 1: Sketch of the (a) standard (fully-baffled) and (b) atypical (unbaffled) experimental tank with marked dimensions and the simulated part of the vessel highlighted; (c) experimental Rushton turbine. (d) Summary of the used Rushton turbines with their diameters.

For the measurements in the *standard configuration*, the impeller was positioned axially with the clearance $C_b = 200$ mm from the tank bottom and the cylindrical tank was equipped with four wall baffles of width $B = 40$ mm, see Fig. 1a. In the case of the *atypical configuration*, the impeller was placed eccentrically and close to the tank bottom, with the clearance $C_u = 10$ mm, eccentricity $E = 100$ mm, and the angle $\alpha = 22.5°$ between the impeller and tank axes. The impeller position was chosen to simulate the geometry of the magnetically driven impellers, consult Fig. 1b.

Mixing time evaluation The batch conductivity measurements were used to evaluate the mixing times. An ionic tracer - saturated solution of sodium chloride - was injected into the tank and its distribution in the vessel's volume was monitored using custom-made conductivity probes placed at three different positions. The specific positions of the probes varied to provide a representative measurement in the vessel; one of the probes was always placed close to the liquid surface, and one was close to the impeller. The measurement itself is based on a linear connection between the conductivity signal κ and the tracer concentration c [9]. Specifically, for the i-th probe pr_i placed at $\boldsymbol{x}_{\mathrm{pr}_i}$, it is possible to evaluate the homogeneity index I_{pr_i}

$$I_{\mathrm{pr}_i}(t) = 1 - \frac{|c(t, \boldsymbol{x}_{\mathrm{pr}_i}) - c_\infty|}{|c_\infty - c(0, \boldsymbol{x}_{\mathrm{pr}_i})|} = 1 - \frac{|\kappa(t, \boldsymbol{x}_{\mathrm{pr}_i}) - \kappa_\infty|}{|\kappa_\infty - \kappa(0, \boldsymbol{x}_{\mathrm{pr}_i})|}, \quad c_\infty = \frac{1}{V_{\mathrm{tank}}} \int_{V_{\mathrm{tank}}} c \, dV \,. \tag{1}$$

The mixing time θ_{95} marks the time period when $I > 0.95$ everywhere in the vessel. However, for the evaluation of the measured conductivity data and to filter-out the signal noise, the θ_{95} was defined as the time period after which I did not fall below 0.95 in two consequent measurements, i.e., within one second, for all the probes.

3 Mathematical model

System governing equations To replicate the performed experiment in a computationally feasible manner, we prepared its digital twin based on the Reynolds-averaged variant of the Navier-Stokes equations coupled with the standard transport equation utilized to simulate the tracer mixing in a pre-computed velocity field. The impeller rotation was accounted for via the standard Multiple Reference Frame (MRF) approach [10]. As a turbulence closure model, the standard $k-\epsilon$ model [11] with the default values of model coefficients was chosen. Consequently, the considered flow governing equations are

$$\begin{aligned} \nabla \cdot (\overline{\boldsymbol{u}} \otimes \overline{\boldsymbol{u}}_R) + \boldsymbol{\omega} \times \overline{\boldsymbol{u}} &= -\frac{1}{\rho}\nabla \overline{p} + \nabla \cdot (\nu_{\text{eff}} \nabla \overline{\boldsymbol{u}}) \\ \nabla \cdot \overline{\boldsymbol{u}} &= 0 \end{aligned} \tag{2}$$

where $\overline{p}$ is the pressure, ρ density, $\overline{\boldsymbol{u}}$ and $\overline{\boldsymbol{u}}_R$ are the absolute velocity in the inertial frame and the relative velocity in the relative frame R, respectively. Next, $\boldsymbol{\omega}$ is the angular velocity of the frame R relative to the angular velocity of the inertial frame and $\overline{\boldsymbol{u}} = \overline{\boldsymbol{u}}_R + \boldsymbol{\omega} \times \boldsymbol{r}$ with $\boldsymbol{r}$ being the position vector. The bars over the symbols denote the Reynolds-averaged variables and will be omitted from now on. The fluid effective kinematic viscosity is computed as $\nu_{\text{eff}} = \nu + \nu_{\text{t}}$, where ν_{t} is the turbulent viscosity provided by the turbulence closure model.

The utilized standard transport equation is formulated with the assumption of Fickian diffusion and takes the form

$$\frac{\partial c}{\partial t} + \nabla \cdot (\boldsymbol{u} c) = \nabla \cdot (D_{\text{eff}} \nabla c)\,, \quad D_{\text{eff}} = D + D_{\text{t}}\,, \tag{3}$$

where c is the tracer volumetric concentration, $\boldsymbol{u}$ is the velocity obtained by solving (2), and D_{eff}, D and D_{t} are, in order, the effective, mass and turbulent diffusivity. The turbulent diffusivity is computed from

$$D_{\text{t}} = \frac{\nu_{\text{t}}}{\text{Sc}_{\text{t}}}\,, \tag{4}$$

where Sc_{t} is the turbulent Schmidt number. Similar to the turbulent viscosity ν_{t}, Sc_{t} is not a fluid property but describes the component transport via turbulent flow [12]. The value of the turbulent Schmidt number is determined experimentally and for stirred vessels, it varies from 0.1-1.5 [13], depending on the vessel geometry.

Computational domain, boundary and initial conditions, used methodology The computational domain was created to mirror the real geometry of the experimental setup. The domain corresponds to the part of the stirred vessel filled with water, see the gray rectangle in Fig. 1b. Both the tank wall and the impeller were 3D modeled and converted into triangulated surfaces, which were later utilized to generate the computational mesh using the OpenFOAM's built-in tool snappyHexMesh. The final mesh with close-ups on MRF zone and impeller is depicted in Fig. 2. Note that the mesh is locally refined close to the tank walls, around the impeller and in the vicinity ofthe boundary between the rotating and stationary zones.

The computational domain boundary is split into following parts: tank wall, impeller and baffles, and liquid surface. Tank wall, impeller and baffles are all considered to be walls with the standard no-slip boundary condition for velocity, and zero gradient in the patch-normal direction for concentration and pressure. Furthermore, for the turbulent quantities k, ϵ and ν_{t}, we utilize standard wall functions [14]. The water surface is simulated as a free surface boundary. The symmetry boundary condition is applied for all the variables as a simplification allowing for single-phase computations.

The flow computations are steady-state ones and fluid at rest is considered as an initial guess. The initial conditions for concentration in the subsequent calculations of tracer transport comprise

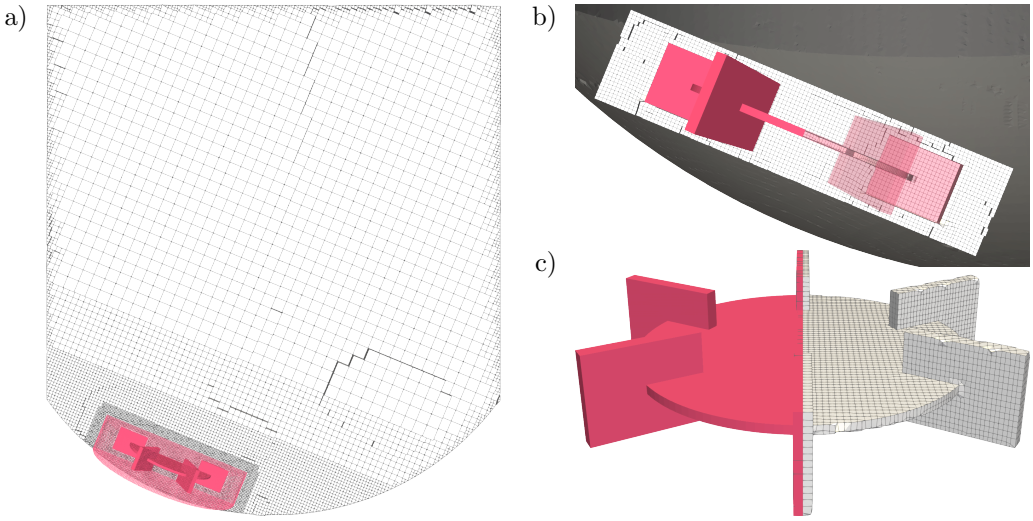

Figure 2: (a) Slice through the computational mesh with the impeller and MRF zone highlighted; (b) Detail of the MRF zone placement and mesh structure; (c) Mesh conformity to the original impeller shape.

a box of volume $V_{c_0} = 8\,\mathrm{cm}^3$ placed outside of the central vortex, see Fig. 5a, and containing such an amount of the tracer that $c_\infty \approx 1$ in the tank.

The flow governing equations (2) were solved using the standard simpleFoam solver from the OpenFOAM library, which utilizes the SIMPLE algorithm [8]. Similarly, the transport equation for c (3) was solved via the scalarTransportFoam solver available in OpenFOAM. However, the standard scalarTransportFoam had to be extended by the treatment of turbulent diffusivity.

Mixing time computation The mixing time θ_{95} is computed based on relation (1). In particular, the homogeneity index is tracked using virtual probes placed at the same locations within the vessel as the experimental ones. The only difference in I evaluation between the experiment and simulation lies in the fact that the tracer concentrations are directly available in the simulation.

4 Results and discussion

4.1 Experimental results

The mixing characteristics were measured for both standard and atypical configurations. In the standard configuration, the mixing time was measured for all three Rushton turbines and the liquid heights $H/T \in \{1.1; 1.5\}$. The measured data were fitted using the following correlation:

$$\theta_{95}^* = \frac{3.0}{N\,\mathrm{Po}^{1/3}} \left(\frac{T}{D}\right)^{2.5} \left(\frac{H}{T}\right)^{0.5} \pm 12\% \,, \quad \mathrm{Po} = \frac{P}{\rho N^2 D^5} \,, \tag{5}$$

where T, D, and H are the above-defined tank and impeller diameters and liquid level (height), respectively. Next, N is the impeller rotational speed in revolutions per second (rps) and Po is the power number with P being the power.

For the atypical configuration, the θ_{95} measurements were performed for the liquid heights of 0.24, 0.34, 0.44, 0.55, 0.6 and 0.65 m, corresponding to the range of the H/T ratio from 0.6 to 1.66. During the experiments, we could still observe the central vortex creation. In order to visualize around 200 data points collected (considering different turbines and rotational speeds), we depict the measurements as the mean ratio of the measured mixing time $\theta_{95}^{\mathrm{exp}}$ and the mixing time θ_{95}^* estimated from correlation (5), which for the standard baffled configuration has the accuracy of $\pm 12\%$. This allows us to compare the mixing time in the unbaffled and standard configurations. The values are depicted in Fig. 3a.

For H/T up to 1.2, the ratio between the measured and predicted data is ~ 1 and the central vortex does not prevent efficient mixing. However, for higher H/T ratios, we observe a significant

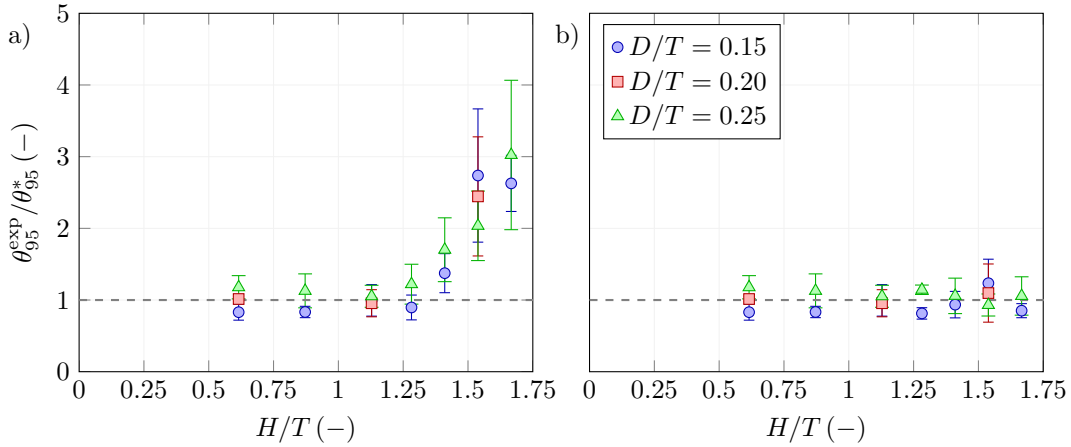

Figure 3: The comparison of measured data for atypical configuration and predicted data for different liquid heights. (a) correlation (5), (b) updated correlation (6).

increase in $\theta_{95}^{\mathrm{exp}}$ compared to the values obtained from (5). Consequently, we propose the following alternation to (5)

$$\theta_{95}^{*} = \begin{cases} \dfrac{3.0}{N\,\mathrm{Po}^{1/3}} \left(\dfrac{T}{D}\right)^{2.5} \left(\dfrac{H}{T}\right)^{0.5} & H/T \leq 1.2 \\ \dfrac{1.2}{N\,\mathrm{Po}^{1/3}} \left(\dfrac{T}{D}\right)^{2.5} \left(\dfrac{H}{T}\right)^{4.5} & H/T > 1.2 \end{cases} \tag{6}$$

which fits well all the data measured in the unbaffled configuration, see Fig. 3b.

4.2 Computational results

Mesh size independence study The study was performed for the flow in a stirred tank with $H/T = 1.1$, eccentrically positioned impeller and rotational speed $N = 5$ rps. The mesh size was varied by changing the size of unrefined cubical base mesh cells. In particular, base mesh cell sides Δ_x of 10, 15, 20 and 25 mm were tested. The variable of interest was selected to be the volume average of turbulent viscosity in the tank, ν_{t}^{*}. The difference between ν_{t}^{*} for $\Delta_x = 10$ mm and $\Delta_x = 20$ mm is less than 3% but the computational time is almost 10 times higher. Therefore, the base-cell size of 20 mm was chosen for further calculations.

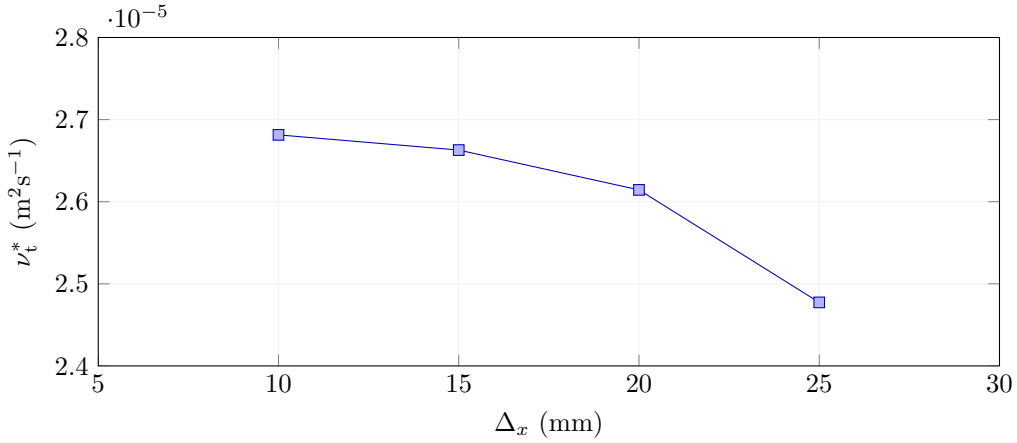

Figure 4: Results of the mesh size independence study for flow.

CFD model sensitivity with respect to turbulent Schmidt number In a standard manner, we assume the turbulent diffusivity D_{t} to be directly proportional to the turbulent viscosity ν_{t} with the turbulent Schmidt number Sc_{t} being (i) the inverse of the proportionality constant,

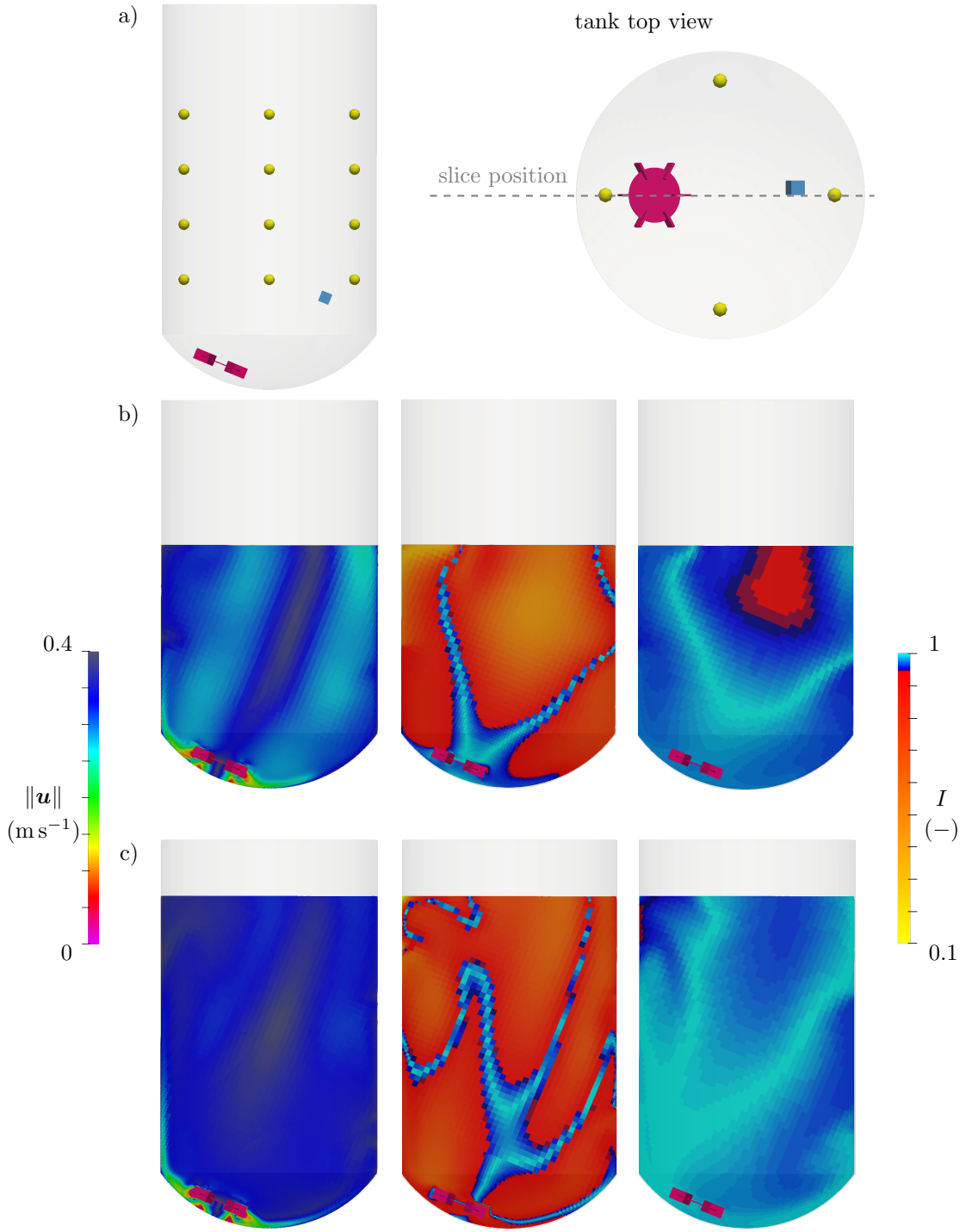

Figure 5: (a) Model of the stirred vessel with measuring probes (yellow), tracer position at $t = 0\,\mathrm{s}$ (blue), and impeller (red); (b) $H/T = 1.1$; from left to right: velocity field, homogeneity index I distribution at $t = \theta_{95}/2$, I at $t = \theta_{95}^{\mathrm{sim}} = 47\,\mathrm{s}$; (c) $H/T = 1.5$; same as (b), $\theta_{95}^{\mathrm{sim}} = 65\,\mathrm{s}$.

see (4), and (ii) a free parameter that has to be calibrated on experimental data. In Fig. 5, we show slices through the model geometry colored by contours of the velocity magnitude and homogeneity index. The slice position in the model geometry as well as the initial box containing the tracer at $t = 0$ s and the locations of the probes are depicted in Fig. 5a. The given velocity fields are stationary and the homogeneity index is shown at $t = \theta_{95}/2$ and $t = \theta_{95}$. The listed results were computed for $N = 1.5$ rps, $D = 100$ mm and $\mathrm{Sc_t} = 0.7$, which is the usually recommended value for standard stirred vessels [6].

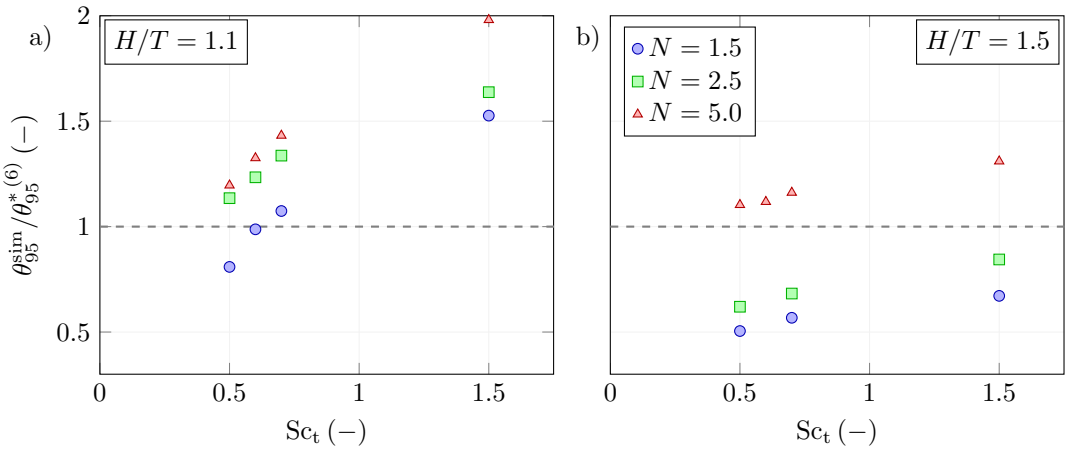

Figure 6: The comparison of simulated data for atypical configuration and predicted data for different Schmidt numbers.

Following the experiments, the impeller diameter of 100 mm and the height ratios $H/T \in \{1.1; 1.5\}$ were used in combination with $\mathrm{Sc_t} \in \{0.5; 0.6; 0.7; 1.5\}$ to determine the model sensitivity with respect to $\mathrm{Sc_t}$, i.e. to its free parameter. Similarly to the experimental results, the calculated data are depicted as the mean ratio of the mixing time estimated from CFD, $\theta_{95}^{\mathrm{sim}}$, and the mixing time obtained from correlation (6), $\theta_{95}^{*(6)}$. Results shown in Fig. 6 demonstrate that $\mathrm{Sc_t}$ required to fit the experimental data varies depending on both the rotational speed N and the height of the liquid. Furthermore, the sensitivity of $\theta_{95}^{\mathrm{sim}}$ on $\mathrm{Sc_t}$ changes in dependence on H/T.

Such results directly contradict the findings for the standard configurations available within the literature [6]. Apparently, the optimal value of $\mathrm{Sc_t}$ in the atypical configuration decreases with the increasing specific power input P/V, where V is the tank volume. This could indicate either an incorrect distribution of turbulent quantities in the vessel volume, or an increasing importance of turbulent diffusivity at higher power inputs. Following the latter hypothesis and examining velocity profiles in Fig. 5 the observed primary vortex is significantly more pronounced for $H/T = 1.1$ than for $H/T = 1.5$. At the same time, $\theta_{95}^{\mathrm{sim}}$ as evaluated from the probes for $H/T = 1.1$ and $\mathrm{Sc_t} = 0.7$ is close to the experimental values. For $H/T = 1.5$, a significantly higher $\mathrm{Sc_t}$ would be needed to fit the experimental data. Such an observation is in contradiction with the assumption of the flow similarity between the standard and the atypical configuration increasing with increasing H/T, i.e. decreasing P/V and, simultaneously, the primary vortex importance. Clearly, further research is required to provide a reliable method for modeling atypical vessel configurations.

5 Conclusion

The presented work is a first step towards the creation of a reliable and computationally efficient model of a stirred tank with an atypical configuration. The developed model is based on the Reynolds-averaged, i.e., semi-phenomenological, approach to modeling the turbulence effects on mixing. Hence, the development started by analyzing custom conductometric experiments. For the atypical configuration, the measurements revealed a dependency of the mixing time on the ratio between the liquid level (height) and the tank diameter that was not observed in the standard baffled configuration. A novel correlation was proposed that fits well all the experimental data, i.e., measurements for all the tested impeller diameters and rotational speeds, and liquid levels. Comparing the correlation-based mixing time estimates to our computational model results, it

was found that the model results are (i) strongly sensitive to the choice of the turbulent Schmidt number Sc_t, and (ii) no single Sc_t can be found to calibrate the model on the available experimental data. The second finding is in direct opposition to the published data available for the standard baffled configuration. Thus, in the following work, we will concentrate on the physics of mixing in unbaffled vessels configurations and study the dependence of Sc_t on the process conditions.

Acknowledgment

This work was supported by the grant of *Specific University Research A1 FCHI 2023 005*, by the institutional support RVO:61388998, and by the Institute of Hydrodynamics of the Czech Academy of Sciences.

References

[1] Barabash, V., Abiev, R. S. & Kulov, N.: Theory and practice of mixing: A review. *Theoretical Foundations of Chemical Engineering*. vol. 52 no. 4: (2018). pp. 473–487.

[2] Busciglio, A., Grisafi, F., Scargiali, F. & Brucato, A.: Mixing dynamics in uncovered unbaffled stirred tanks. *Chemical Engineering Journal*. vol. 254: (2014). pp. 210–219.

[3] Ram, K., Vickroy, T. B., Lamb, K. A., Slater, N. K., Dennis, J. S. & Duffy, L. E.: Mixing in process vessels used in biopharmaceutical manufacturing. *Biotechnology progress*. vol. 16 no. 2: (2000). pp. 244–247.

[4] Matcon, Ltd. Magnetic coupled mixer for pharmaceuticals & biotech: (2022). URL `https://www.steridose.com/products/magnetic-coupled-mixers`. accessed 20.12.2022.

[5] Yu, Z., Finch, B. A. & Hale, D. A.: Mixing of stratified miscible liquids in an unbaffled tank with application in high concentration protein drug product manufacturing. *Industrial & Engineering Chemistry Research*. vol. 57 no. 9: (2018). pp. 3397–3409.

[6] Galletti, C., Pintus, S. & Brunazzi, E.: Effect of shaft eccentricity and impeller blade thickness on the vortices features in an unbaffled vessel. *Chemical Engineering Research and Design*. vol. 87 no. 4: (2009). pp. 391–400.

[7] Campolo, M. & Soldati, A.: Numerical evaluation of mixing time in a tank reactor stirred by a magnetically driven impeller. *Industrial & engineering chemistry research*. vol. 43 no. 21: (2004). pp. 6836–6846.

[8] Openfoam v8: (2022). URL `https://openfoam.org/version/8/`. accessed 13.12.2022.

[9] Landau, J. & Prochazka, J.: Studies on mixing. xi. experimental methods for following the homogenation of miscible liquids by rotary mixers. *Collection of Czechoslovak Chemical Communications*. vol. 26 no. 8: (1961). pp. 1976–1990.

[10] MRF development: (2022). URL `https://openfoamwiki.net/index.php/See_the_MRF_development`. accessed 23.12.2022.

[11] Launder, B. E. & Spalding, D. B. The numerical computation of turbulent flows. In *Numerical prediction of flow, heat transfer, turbulence and combustion*: pp. 96–116. Elsevier: (1983).

[12] Menter, F. & Esch, T.: Elements of industrial heat transfer predictions. In *16th Brazilian Congress of Mechanical Engineering (COBEM)*: volume 109: page 650: (2001).

[13] Gualtieri, C., Angeloudis, A., Bombardelli, F., Jha, S. & Stoesser, T.: On the values for the turbulent schmidt number in environmental flows. *Fluids*. vol. 2 no. 2: (2017). page 17.

[14] Darwish, M. & Moukalled, F. *The finite volume method in computational fluid dynamics: an advanced introduction with OpenFOAM® and Matlab®*. Springer: (2021).